Molecular Simulations of $CO_2/N_2/H_2O$ Gaseous Mixture Separation in Graphtriyne Membrane

Noelia Faginas-Lago[1(✉)], Yusuf Bramastya Apriliyanto[2], and Andrea Lombardi[1]

[1] Dipartimento di Chimica, Biologia e Biotecnologie, Università di Perugia, Perugia, Italy
noelia.faginaslago@unipg.it

[2] Department of Chemistry, Bogor Agricultural University, Jl Tanjung Kampus IPB Dramaga, 16680 Bogor, Indonesia

Abstract. Graphynes are porous derivatives of graphene that can be considered as ideal 2D nanofilters. Here, we investigate by theoretical methods graphtriyne single layer, proposing them as membranes featuring pores of subnanometer size suitable for $CO_2/N_2/H_2O$ separation and CO_2 uptake. The potential energy surfaces, representing the intermolecular interactions within the $CO_2/N_2/H_2O$ gaseous mixtures and between the graphtriyne single layer and the molecules, have been formulated in an internally consistent way, by adopting potential models far more accurate than the traditional Lennard-Jones functions, routinely used to predict static and dynamical properties of matter.

Keywords: Molecular dynamics · Empirical potential energy surface · Gaseous separation · Graphtriyne membrane · DL_POLY

1 Introduction

CO_2 concentration in the atmosphere is in a high level and it keeps arising in recent decades due to economic growth reasons in most of countries [1]. Many problems arise from the excess of CO_2, for instance environmental pollution and climate change in connection to the global warming phenomenon [2]. Adsorption using porous materials is a promising way to capture CO_2 generated mostly by fossil fuels combustion, in order to mitigate greenhouse gas effects associated with excessive CO_2 emissions into the atmosphere [3–6]. This method is favoured in terms of its simplicity and low implementation costs than the traditional aqueous chemical absorption [7]. A range of porous materials such as nanoporous carbons [8–10], zeolites and zeolitic imidazolate framework (ZIFs) [11,12], metal-organic frameworks (MOFs) [13], porous polymer networks (PPNs) or also known as covalent organic frameworks/polymers (COFs/COPs) [14,15], and a slurry made of solid adsorbents in a liquid absorbent [16] have been exploited

© Springer Nature Switzerland AG 2019
S. Misra et al. (Eds.): ICCSA 2019, LNCS 11624, pp. 374–387, 2019.
https://doi.org/10.1007/978-3-030-24311-1_27

and reported for CO_2 capture in the past few years. An alternative to porous adsorbing materials is a nanoporous membrane that use a combination of surface adsorption and its intrinsic pores acting as molecular sieving to separate CO_2 from other gaseous mixtures [17].

However, due to the vast number of theoretically applicable materials, in practice it is very difficult or even an impossible task to experimentally synthesize, characterize and evaluate their performance for CO_2 capture and separation of all possible materials [18–20]. Up to this state, computer modelling and simulations play an important role in the material design and development, prior to the experimental stage [3]. A generic force fields like AMBER [21] and UFF [22] often does not have the appropriate parameters when we deal with a particular system, thus parts of the potential energy function have to be developed or refined on purpose, using available theoretical and experimental data. Although force fields parameterization is a delicate task, the development of force fields is an indispensable work. In the last years, various force fields have specifically been developed for evaluating gaseous adsorption in porous carbons, graphene and its derivatives [23–25] MOFs [26,27], zeolites [28] and other polymeric materials [29] to quantitatively describe molecular interactions providing realistic predictions of relevant adsorption dynamics and transport properties of gas under consideration. Recently, carbon-based membranes emerge as potential materials because of their exceptional properties (e.g. hydrophobic, chemically inert and thermally stable) are economically suitable and viable for post combustion CO_2 capture and separation [29,30]. MOFs and polymers for instance, although they exhibit good selectivity and permeability, they are susceptible to heat and water vapour which is a characteristic of post combustion flue gas. Permeability and selectivity are two main aspects to determine whether a membrane can be effective for gas separation. It is already known that permeability is inversely proportional to the thickness of the membrane. Therefore, single atom thick planar membrane may have great potential for gas separation [31]. γ-graphynes are single atomic layers belonging to the class of carbon allotropes where the carbon atoms are arranged as a function of the C-C triple bonds bridging two adjacent hexagons. γ-graphynes exhibit similar properties with graphene, but the pores are uniformly distributed and adjustable [32]. Moreover, γ-graphynes have lower dispersion forces that minimalize aggregates formation among graphyne molecules. Synthesis and characterization techniques of graphyne are actively being developed in the last years [33]. Force fields related to gas adsorption on γ-graphynes have also been developed and tested on accurate ab initio calculations in our previous works [34–37]. Therefore, in this report, extended molecular dynamics (MD) simulations were performed on a wide range of conditions of applied interest in post combustions; involving $CO_2/N_2/H_2O$ gaseous mixtures separation [38] in graphtriyne membrane (a form of γ-graphynes, in which each phenyl ring is connected through three acetylenic bonds placed as a bridge).

On an other hand, Molecular Dynamics (MD) simulations is a theoretical powerful tool to analyze extensively the structural rearrangement of pure solvents, solution mixtures and the combustion processes [39–45]. Combustion is a

complex of chemical and physical nature of the process that leads to the conversion of chemical energy into heat energy stored in fuels. From a molecular point of view, the combustion is the result of numerous elementary processes, chemical reactions including mono-, bi- and ter-molecular and energy-transfer processes (which ensure the distribution of the energy released by the exothermic reactions to everything the system) [46–49].

The paper is organized as follows: in Sect. 2, we outline the methods and the construction of the potential energy function. We give in Sect. 3 the details of preliminary results and in Sect. 4 concluding remarks are given.

2 Methods

The MD simulations were performed in the simulation box of 72.210 Å × 62.523 Å× 280.0 Å. Each box consists of graphtriyne membrane with dimensions of 72.210 Å× 62.523 Å placed in the middle of the box. Four different temperatures (333, 353, 373 and 400 K) were employed for the simulations of $CO_2/N_2/H_2O$ gaseous mixture with equal composition of CO_2, N_2 and H_2O. The structures of graphtriyne membranes were taken from Ref. [50], where the structures had been optimized using periodic DFT calculations. A H_2O model reported in Ref. [51] was implemented with the charge distributions correspond to the dipole moment of water in gas phase (1.85 D) [52], while a three-charge-site N_2 model [53] and a five-charge-site CO_2 model [54] were adopted to account for the quadrupole moment (See Fig. 1).

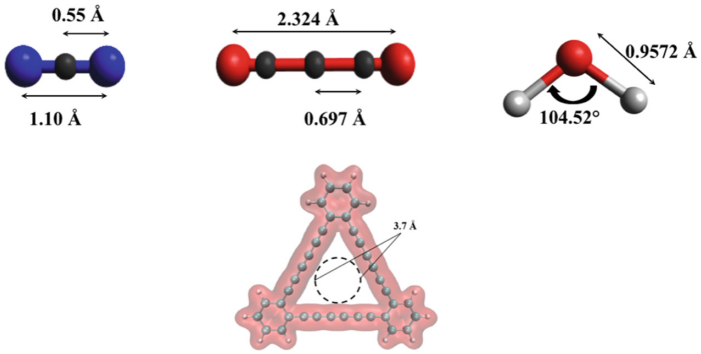

Fig. 1. The models used to represent nitrogen, carbon dioxide and water. Unit pore of graphtriyne represented by the electron density plot of its smallest molecular precursor. The dashed circle depicted inside the triangular pore correspond to its effective pore with a diameter of about 3.7 Å.

The intermolecular forces between the gas molecules, and between the gas molecules and the membranes were expressed using the Improved Lennard-Jones (ILJ) potential [55–59].

$$V_{ILJ}(r) = \varepsilon \left[\frac{m}{n(r) - m} \left(\frac{r_0}{r} \right)^{n(r)} - \frac{n(r)}{n(r) - m} \left(\frac{r_0}{r} \right)^{m} \right] \quad (1)$$

In Eq. 1, ε, r_0 and m are pair specific parameters and r is the distance between the positions of the two interacting centers placed on different molecules. The first term of the bracketed sum in Eq. 1 (the positive one) represents the size-repulsion contribution arising from each pair, while the second term (negative) represents the effective dispersion attraction contribution for the given pair of centers. The exponent $n(r)$ of the first term modulates the falloff of the repulsion and controls the strength of the attraction as a function of r as follows:

$$n(r) = \beta + 4.0 \left(\frac{r}{r_0} \right)^2 \quad (2)$$

with β being an adjustable parameter able to modulate the hardness of the interaction [60,61]. The introduction of this modulating parameter (not present in the standard Lennard-Jones function (LJ)) provides ILJ with the possibility of indirectly taking into account some effects of the induction, charge transfer and atom clustering. The parameter β also corrects the dependence of the interaction on the internuclear distance, improving the LJ function in the asymptotic region. For a full account of the advantages of the ILJ function see Refs. [62–65] and references therein and also parallel studies for the construction of expansion basis sets for the quantum mechanical treatment of N-body problems of practical interest for intermolecular and intramolecular and reactive dynamics of polyatomic molecules and clusters [66–69]. In the interactions between neutral molecules m is set equal to 6.

All of the ILJ parameters used in this report was improved and tested in comparison with high level ab initio calculations Ref. [35,50]. The cutoff distance for the ILJ and electrostatic interactions is 15 Å, where the Ewald method was applied for the calculation of electrostatic interactions. All molecular dynamics simulation were performed using DL_POLY program [70] in the canonical (NVT) ensemble employing the Nose-Hoover thermostat with periodic boundary conditions in all directions. Each simulation was performed for 5.5 ns after 0.5 ns equilibration period with a fixed timestep of 1 fs, where the statistical data and trajectory were collected every 2 ps.

Seven different amounts of gas have been loaded into the simulation box for every system to investigate the influence of pressure in our simulations. The gas pressure was computed using the Peng-Robinson equation of state [71]. In order to mimic post-combustion conditions, the initial pressures were chosen at relatively low pressure, under 5.5 atm. The gas molecules were randomly distributed with equal amount into the two regions of box, thus there is no pressure gradient inside the box (Fig. 2). The membranes were considered as a frozen framework and the gas molecules were treated as rigid bodies. The gas molecules could cross the membrane multi times at both directions during the simulation. The number of permeation events was then monitored along with the z-density and radial distribution function profiles. All graphical representations of the molecular trajectories were processed using VMD package [72].

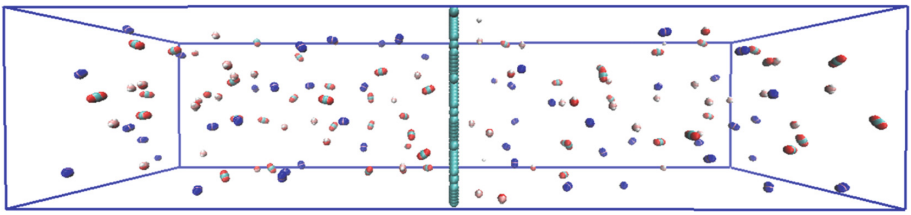

Fig. 2. The simulation box filled with gaseous mixture of CO_2, N_2 and H_2O. The cyan layer in the middle of the box is the graphtriyne single layer.

3 Results and Discussion

3.1 Gas Permeability

Production run of every simulation was initialized after the equilibration step. The number of permeation events occurred during the production run was counted and then plotted against the simulation time. The slope of this plot is an estimation of the gas permeation rate measured in a unit of molecules ps^{-1} (Fig. 3). Using this data, the gas permeance was then calculated by dividing the permeation rate with the corresponding pressure and area of the membrane. Gas permeances were reported in Fig. 4 using gas permeance unit (GPU), where 1 GPU is equal to 3.35×10^{-10} mol m^{-2} s^{-1} Pa^{-1}. Figure 4, left panel, shows that N_2 permeances are slightly affected by the pressures. Meanwhile, CO_2 and H_2O permeances are high at low pressure and relatively flat at higher pressures. However, for all gas molecules, their permeances do not vary much at pressures higher than 1 atm. Using this flat region, we calculated the average of gas permeance for each gas and plotted it as a function of temperature (Fig. 4, right panel).

Right panel of Fig. 4 shows that the average of gas permeance for all gas decreases with increasing of temperature. This phenomenon is related to the kinetic energy of molecules; the higher is the kinetic energy, the higher is the velocity of molecules to compete with attraction forces of the membrane. Therefore, high temperature decrease gas permeance by lowering attraction effect to steer molecules toward the membrane. The penetration process encounters energy barriers when CO_2 molecules approach membrane in parallel configurations [35]. This qualitatively explains why CO_2 molecules are more difficult to pass through the membrane even though the amounts of CO_2 molecules attracted and adsorbed by the membrane are larger than those of H_2O (can be seen in the z-density profiles, will be discussed later). Therefore, as can be seen in the Fig. 4, H_2O permeances are higher than those of CO_2 and N_2.

Furthermore, we calculated permeance selectivities as ratio between average of gas permeance and plotted the values as function of temperature (Fig. 5). Indeed the permeance selectivity depends on the temperature, but in general, the trend lines are relatively flat if we consider also the deviation error. Permeance selectivity of H_2O/N_2 is higher than CO_2/N_2 and H_2O/CO_2. Meanwhile,

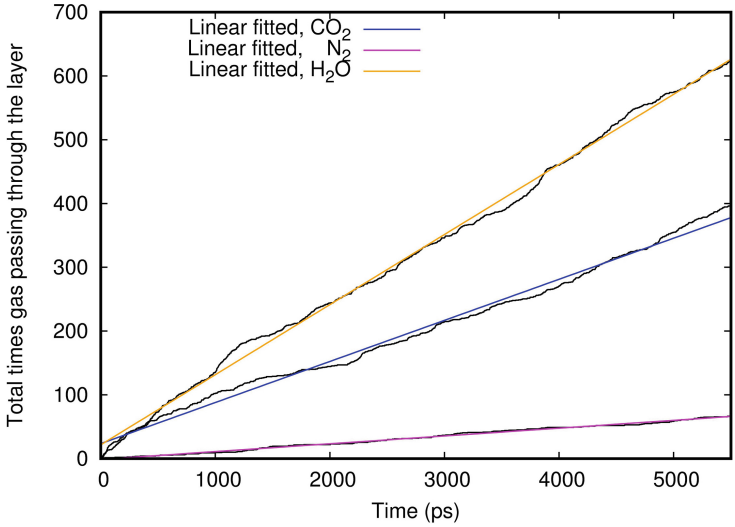

Fig. 3. The number of permeation events as a function of simulation time for single layer at 4.62 atm and 333 K.

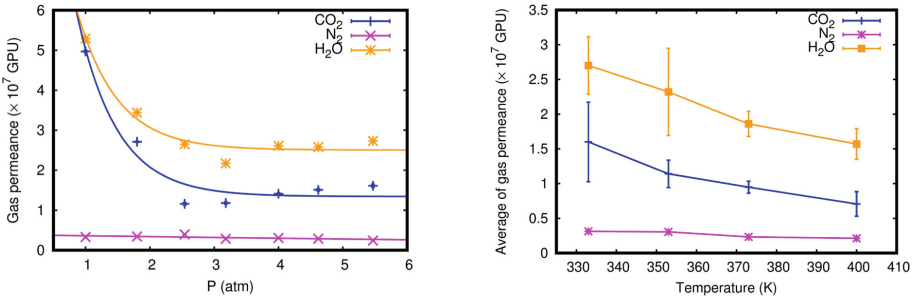

Fig. 4. Gas permeance of the single layer system at 333 K (left panel) and average of gas permeance of the single layer system as a function of temperature (right panel).

H_2O/CO_2 selectivity is around 2 which can be interpreted as the membrane is not selective enough for CO_2/H_2O separation. The CO_2 permeances (ranging from 1.0 to 2.0×10^{-7} GPU) are two order of magnitudes higher than those reported by Liu et al. [17] (2.8×10^{-5} GPU) for nanoporous graphene at 300 K and by Schrier [14] (3×10^{-5} GPU) for porous graphene (PG-ES1) at 325 K. However, the CO_2/N_2 permeance selectivities are lower than those reported by Liu et al. [17] and Schrier [14] (about 100 and 60 respectively).

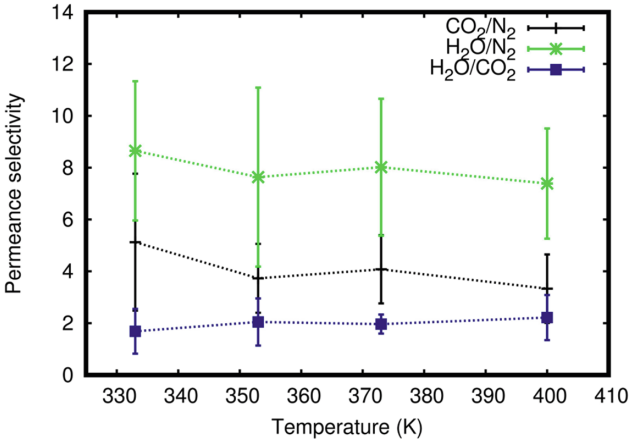

Fig. 5. Permeance selectivity for single layer system.

3.2 Gas Adsorption

The gas adsorption is reflected by the mean number of gas along the z-axis, perpendicular with the graphtriyne, denoted as z-density profiles ρ(z). The z-density profiles of single layer system peak at a distance of around 3.4 Å from the surface for all gas molecules (Fig. 6, left panel). The stronger CO_2 attraction can be seen in the z-density profiles, where CO_2 has highest peaks. We can also see from the radial distribution function (Fig. 6, right panel) that CO_2 has highest probability to be located near to the carbon atom of graphtriyne (around 4 Å) than the other gas molecules. High peaks of CO_2 in the z-density profiles and the radial distribution functions correspond to the deep and wide of CO_2 potential well, meaning a strong long ranged attractions. As already discussed in the previous section, the permeation events are closely related to the adsorption of gas over the surfaces of membranes. The more molecules are adsorbed, the higher is their permeances. However, the stereodynamic requirements of CO_2 for crossing the membrane lead to lower permeances than those of H_2O.

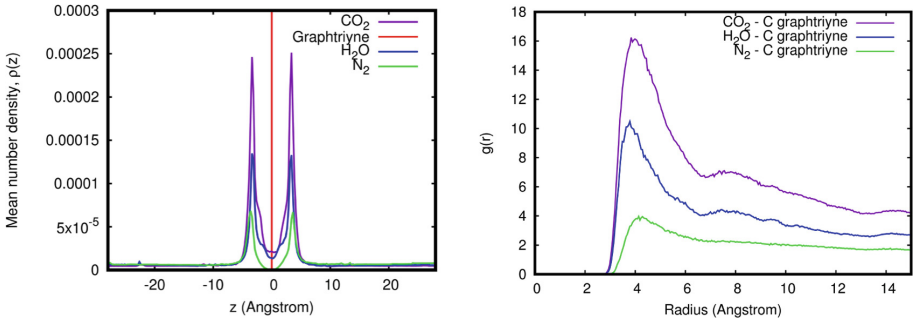

Fig. 6. z-Density profile (left panel) and radial distribution function (right panel) of the single layer system at 1 atm and 353 K.

We calculated the gas uptake by integrating the area under peaks of the z-density profiles. This area is considered as the adsorption region located in the range of ±6.9 Å with respect to the membrane position. Notice that, the z-density does not peak at the centre of the pore, place with the lowest potential energy. This feature of z-density had already been well-discussed in our previous report [35]. The gas uptakes for all applied pressures were presented in left panel of Fig. 7 as the adsorption isotherms. We can see that the gas uptake is linearly related to the initial pressure; the higher is the initial pressure applied, the higher is the gas uptake value. Therefore, using linear regression, we can estimate the adsorption coefficient from the slope of the linearly fitted isotherm adsorption. The adsorption coefficient for all gas molecules are reported in the right panel of Fig. 7 as a function of temperature. It can be seen from Fig. 7 that CO_2 has the highest gas uptakes and adsorption coefficients among gas molecules. On the other hand, despite H_2O has the highest permeance, its gas uptakes and adsorption coefficients are low, confirming weaker attraction forces than those of CO_2. Weak attraction of N_2 by the membrane is manifested by the fact that N_2 has the lowest adsorption coefficient (about 0.06 to 0.07 mmol g^{-1} atm^{-1}). Figure 7 (right panel) shows that in general, the adsorption coefficients decrease as the increasing of temperature. Obviously, higher temperature implies higher mobility of gas molecules inside the simulation box, thus gas physisorption is ineffective at relatively high temperature.

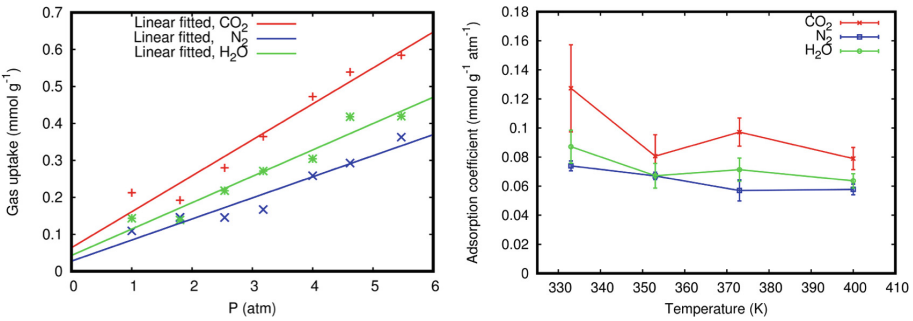

Fig. 7. Adsorption isotherm of the single layer system at 373 K (left panel) and adsorption coefficient plotted as a function of temperature for the single layer system (right panel).

The total adsorption selectivites were plotted in Fig. 8 and the full data are given in Table 1.

The CO_2/N_2 selectivities reported in Table 1 are higher than those reported in our previous report [35]. However, the gas uptake values and the corresponding adsorption coefficients are relatively lower than those obtained in the previous work. It is obvious that this difference comes from different kind of gaseous mixtures and conditions applied in the simulations. Therefore, with all advantages of carbon-based materials for postcombustion CO_2 capture and separation, graphtriyne layer is one of the most promising alternative of carbon-based membranes.

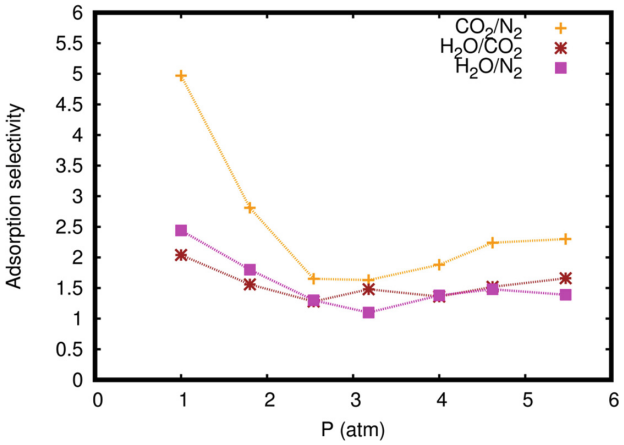

Fig. 8. Adsorption selectivity of gas at 333 K for the single layer system.

Table 1. Adsorption selectivity of $CO_2/N_2/H_2O$ gaseous mixture for single layer system.

Temperature (K)	Gas	Adsorption selectivity						
		1.00 atm	1.80 atm	2.54 atm	3.18 atm	4.00 atm	4.62 atm	5.47 atm
333	CO_2/N_2	4.97	2.81	1.65	1.63	1.88	2.24	2.30
	H_2O/N_2	2.44	1.80	1.30	1.10	1.38	1.48	1.39
	CO_2/H_2O	2.04	1.56	1.28	1.48	1.36	1.52	1.66
353	CO_2/N_2	4.43	1.53	2.43	1.78	1.63	1.73	1.70
	H_2O/N_2	2.10	1.40	1.21	1.13	1.11	1.19	1.25
	CO_2/H_2O	2.11	1.09	2.01	1.57	1.46	1.45	1.35
373	CO_2/N_2	2.30	1.34	2.07	2.37	1.97	1.98	1.70
	H_2O/N_2	1.38	0.95	1.56	1.70	1.20	1.48	1.17
	CO_2/H_2O	1.67	1.44	1.33	1.40	1.65	1.34	1.45
400	CO_2/N_2	2.66	2.23	1.71	1.96	1.83	1.53	1.69
	H_2O/N_2	1.05	1.72	0.98	1.39	1.25	1.17	1.13
	CO_2/H_2O	2.53	1.30	1.74	1.41	1.46	1.31	1.50

4 Conclusions

The performance of graphtriyne-based membranes for $CO_2/N_2/H_2O$ separation has been investigated by extensive MD simulations based on a new formulation of the force fields required to describe the interactions in gas phase and between the molecules and the layer. The model is a quantitative tool for the estimation of membrane properties, such as gas uptake, permeance, and selectivity in view of

applications for postcombustion mixture separation and can be easily extended to carbon nanostructures interacting with a variety of different gaseous mixtures. Based on the molecular simulation results, we found that graphtriyne have a high permeance (and relatively good selectivity in comparation with other carbon-based separating membranes; the order of magnitude of 10^{-7}GPU). Despite single layer graphtriyne is not selective for CO_2-H_2O separation, it is relatively selective for CO_2-N_2 and H_2O-N_2 separation with permeance selectivity of 2.01 to 7.76 for CO_2/N_2; 5.26 to 11.33 for H_2O/N_2 (depending on the applied temperature). Permeation and adsorption depend on the applied temperature; high temperature decrease permeation and adsorption. These results suggest that graphtriyne exhibit good performance as an initial molecular sieve candidate for postcombustion CO_2 capture and separation achieved through combination of surface adsorption and its intrinsic pores.

Acknowledgement. The authors thank MIUR and Perugia University for financial support through the AMIS project ("Dipartimenti di Eccellenza-2018–2022"). AL thanks the Italian MIUR for funding through the program PRIN 2015 (contract 2015F59J3R 002). AL and NFL also thanks the Dipartimento di Chimica, Biologia e Biotecnologie for funding under the program Fondo Ricerca di Base 2017. AL and NFL also thank the OU Supercomputing Center for Education & Research (OSCER) at the University of Oklahoma (OU) for allocated computing time. YBA thanks to the LCPQ - Université de Toulouse III for allocated computing time.

References

1. (EPA), U.S. Environmental Protection Agency: Climate Change Indicators in the United States: Global Greenhouse Gas Emissions (2016)
2. (WRI), World Resources Institute: Climate Analysis Indicators Tool (CAIT) 2.0: WRI's Climate Data Explorer
3. Huck, J.M., et al.: Evaluating different classes of porous materials for carbon capture. Energy Environ. Sci. **7**, 4132–4146 (2014)
4. Bui, M., et al.: Carbon capture and storage (CCS): the way forward. Energy Environ. Sci. **11**, 1062–1176 (2018)
5. Li, J.R., et al.: Porous materials with pre-designed single-molecule traps for CO_2 selective adsorption. Nat. Commun. **4**, 1538 (2014)
6. Celiberto, R., et al.: Atomic and molecular data for spacecraft re-entry plasmas. Plasma Sour. Sci. Technol. **25**(3), 033004 (2016)
7. Smit, B.: Carbon capture and storage: introductory lecture. Faraday Discuss. **192**, 9–25 (2016)
8. Srinivas, G., Krungleviciute, V., Guo, Z.X., Yildirim, T.: Exceptional CO_2 capture in a hierarchically porous carbon with simultaneous high surface area and pore volume. Energy Environ. Sci. **7**, 335–342 (2014)
9. Ganesan, A., Shaijumon, M.: Activated graphene-derived porous carbon with exceptional gas adsorption properties. Microporous Mesoporous Mater. **220**, 21–27 (2015)
10. Ghosh, S., Sevilla, M., Fuertes, A.B., Andreoli, E., Ho, J., Barron, A.R.: Defining a performance map of porous carbon sorbents for high-pressure carbon dioxide uptake and carbon dioxide-methane selectivity. J. Mater. Chem. A **4**, 14739–14751 (2016)

11. Kim, J., Lin, L.C., Swisher, J.A., Haranczyk, M., Smit, B.: Predicting large CO_2 adsorption in aluminosilicate zeolites for postcombustion carbon dioxide capture. J. Am. Chem. Soc. **134**(46), 18940–18943 (2012)
12. Liu, B., Smit, B.: Molecular simulation studies of separation of CO_2/N_2, CO_2/CH_4, and CH_4/N_2 by ZIFs. J. Phys. Chem. C **114**(18), 8515–8522 (2010)
13. Lin, L.C., et al.: Understanding CO dynamics in metal-organic frameworks with open metal sites. Angew. Chem. Int. Ed. **52**(16), 4410–4413 (2013)
14. Schrier, J.: Carbon dioxide separation with a two-dimensional polymer membrane. ACS Appl. Mater. Interfaces **4**(7), 3745–3752 (2012)
15. Xiang, Z., et al.: Systematic tuning and multifunctionalization of covalent organic polymers for enhanced carbon capture. J. Am. Chem. Soc. **137**(41), 13301–13307 (2015)
16. Liu, H., et al.: A hybrid absorption–adsorption method to efficiently capture carbon. Nat. Commun. **5**, 5147 (2014)
17. Liu, H., Dai, S., Jiang, D.: Insights into CO_2/N_2 separation through nanoporous graphene from molecular dynamics. Nanoscale **5**, 9984–9987 (2013)
18. Lombardi, A., Lago, N.F., Laganà, A., Pirani, F., Falcinelli, S.: A bond-bond portable approach to intermolecular interactions: simulations for N-methylacetamide and carbon dioxide dimers. In: Murgante, B., et al. (eds.) ICCSA 2012. LNCS, vol. 7333, pp. 387–400. Springer, Heidelberg (2012). https://doi.org/10.1007/978-3-642-31125-3_30
19. Lombardi, A., Faginas-Lago, N., Pacifici, L., Costantini, A.: Modeling of energy transfer from vibrationally excited CO_2 molecules: cross sections and probabilities for Kinetic modeling of atmospheres, flows, and plasmas. J. Phys. Chem. A **117**(45), 11430–11440 (2013)
20. Falcinelli, S., et al.: Modeling the intermolecular interactions and characterization of the dynamics of collisional autoionization processes. In: Murgante, B., et al. (eds.) ICCSA 2013. LNCS, vol. 7971, pp. 69–83. Springer, Heidelberg (2013). https://doi.org/10.1007/978-3-642-39637-3_6
21. Pearlman, D., et al.: AMBER. A package of computer-programs for applying molecular mechanics, normal-mode analysis, molecular-dynamics and free-energy calculations to simulate the structural and energetic properties of molecules. Comput. Phys. Commun. **91**, 1–41 (1995)
22. Rappe, A.K., Casewit, C.J., Colwell, K.S., Goddard, W.A., Skiff, W.M.: UFF, a full periodic table force field for molecular mechanics and molecular dynamics simulations. J. Am. Chem. Soc. **114**(25), 10024–10035 (1992)
23. Vekeman, J., García Cuesta, I., Faginas-Lago, N., Wilson, J., Sánchez-Marín, J., Sánchez de Merás, A.: Potential models for the simulation of methane adsorption on graphene: development and CCSD(T) benchmarks. Phys. Chem. Chem. Phys. **20**(18), 25518–25530 (2018)
24. Lombardi, A., Faginas-Lago, N., Pacifici, L., Grossi, G.: Energy transfer upon collision of selectively excited CO_2 molecules: state-to-state cross sections and probabilities for modeling of atmospheres and gaseous flows. J. Chem. Phy. **143**(3), 034307 (2015)
25. Faginas-Lago, N., Albertí, M., Costantini, A., Laganà, A., Lombardi, A., Pacifici, L.: An innovative synergistic grid approach to the computational study of protein aggregation mechanisms. J. Mol. Model. **20**(7), 2226 (2014)
26. Boyd, P.G., Moosavi, S.M., Witman, M., Smit, B.: Force-field prediction of materials properties in metal-organic frameworks. J. Phys. Chem. Lett. **8**(2), 357–363 (2017)

27. Lin, L.C., Lee, K., Gagliardi, L., Neaton, J.B., Smit, B.: Force-field development from electronic structure calculations with periodic boundary conditions: applications to gaseous adsorption and transport in metal-organic frameworks. J. Chem. Theory Comput. **10**(4), 1477–1488 (2014)
28. Lim, J.R., Yang, C.T., Kim, J., Lin, L.C.: Transferability of CO_2 force fields for prediction of adsorption properties in all-silica zeolites. J. Phys. Chem. C **122**(20), 10892–10903 (2018)
29. DuBay, K.H., Hall, M.L., Hughes, T.F., Wu, C., Reichman, D.R., Friesner, R.A.: Accurate force field development for modeling conjugated polymers. J. Chem. Theory Comput. **8**(11), 4556–4569 (2012)
30. Bartolomei, M., Carmona-Novillo, E., Giorgi, G.: First principles investigation of hydrogen physical adsorption on graphynes' layers. Carbon **95**, 1076–1081 (2015)
31. Du, H., Li, J., Zhang, J., Su, G., Li, X., Zhao, Y.: Separation of hydrogen and nitrogen gases with porous graphene membrane. J. Phys. Chem. C **115**(47), 23261–23266 (2011)
32. James, A., et al.: Graphynes: indispensable nanoporous architectures in carbon flatland. RSC Adv. **8**, 22998–23018 (2018)
33. Gao, X., et al.: Ultrathin graphdiyne film on graphene through solution-phase van der Waals epitaxy. Sci. Adv. **4**(7), eaat6378 (2018)
34. Faginas, N., Huarte-Larrañaga, F., Laganà, A.: Full dimensional quantum versus semiclassical reactivity for thebent transition state reaction N + N_2. Chem. Phys. Lett. **464**(4–6), 249–255 (2008)
35. Apriliyanto, Y.B., et al.: Nanostructure selectivity for molecular adsorption and separation: the case of graphyne layers. J. Phys. Chem. C **122**(28), 16195–16208 (2018)
36. Faginas-Lago, N., Yeni, D., Huarte, F., Wang, Y., Alcamí, M., Martin, F.: Adsorption of hydrogen molecules on carbon nanotubes using quantum chemistry and molecular dynamics. J. Phys. Chem. A **120**(32), 6451–6458 (2016)
37. Yeamin, M.B., Faginas-Lago, N., Albertí, M., García Cuesta, I., Sánchez-Marín, J., Sánchez de Merás, A.: Multi-scale theoretical investigation of molecular hydrogen adsorption over graphene: coronene as a case study. RSC Adv. **4**, 54447–54453 (2014)
38. Barreto, P.R., et al.: Potential energy surfaces for interactions of H_2O with H_2, N_2 and O_2: a hyperspherical harmonics representation, and a minimal model for the H_2O-rare-gas-atom systems. Comput.Theor. Chem. **990**, 53–61 (2012)
39. Pallottelli, S., Tasso, S., Pannacci, N., Costantini, A., Lago, N.F.: Distributed and collaborative learning objects repositories on grid networks. In: Taniar, D., Gervasi, O., Murgante, B., Pardede, E., Apduhan, B.O. (eds.) ICCSA 2010. LNCS, vol. 6019, pp. 29–40. Springer, Heidelberg (2010). https://doi.org/10.1007/978-3-642-12189-0_3
40. Lago, N., Laganá, A., Gargano, R., Barreto, P.: On the semiclassical initial value calculation of thermal rate coefficients for the reaction N + N_2. J. Chem. Phys. **125**(11), 114311 (2006)
41. Laganà, A., Faginas Lago, N., Rampino, S., Huarte-Larrañaga, F., García, E.: Thermal rate coefficients in collinear versus bent transition state reactions: the N + N_2 case study. Phys. Scr. **78**(5), 058116 (2008)
42. Rampino, S., Faginas-Lago, N., Laganà, A., Huarte-Larrañaga, F.: An extension of the grid empowered molecular simulator to quantum reactive scattering. J. Comput. Chem. **33**, 708–714 (2012)

43. Laganà, A., Crocchianti, S., Faginas Lago, N., Pacifici, L., Ferraro, G.: A nonorthogonal coordinate approach to atom-diatom parallel reactive scattering calculations. Collect. Czech. Chem. Commun. **68**(2), 307–330 (2003)
44. Faginas Lago, N., Lombardi, A., Pacifici, L., Costantini, A.: Design and implementation of a grid application for direct calculations of reactive rates. Comput. Theor. Chem. **1022**, 103–107 (2013)
45. Lombardi, A., Faginas-Lago, N., Laganà, A.: Grid calculation tools for massive applications of collision dynamics simulations: carbon dioxide energy transfer. In: Murgante, B., et al. (eds.) ICCSA 2014. LNCS, vol. 8579, pp. 627–639. Springer, Cham (2014). https://doi.org/10.1007/978-3-319-09144-0_43
46. Skouteris, D., Balucani, N., Faginas-Lago, N., Falcinelli, S., Rosi, M.: Dimerization of methanimine and its charged species in the atmosphere of Titan and interstellar/cometary ice analogs. Astron. Astrophys. **584**, 8 (2015)
47. Rosi, M., et al.: Possible scenarios for SiS formation in the interstellar medium: electronic structure calculations of the potential energy surfaces for the reactions of the SiH radical with atomic sulphur and S_2. Chem. Phys. Lett. **695**, 87–93 (2018)
48. Podio, L., et al.: Silicon-bearing molecules in the shock L1157-B1: first detection of SiS around a Sun-like protostar. Mon. Not. Roy. Astron. Soc. Lett. **470**(1), 16–20 (2017)
49. Battaglia, S., Faginas-Lago, N., Andrae, D., Evangelisti, S., Leininger, T.: Increasing radical character of large [n]cyclacenes unveiled by wave function theory. J. Phys. Chem. A **121**(19), 3746–3756 (2017)
50. Bartolomei, M., Giorgi, G.: A novel nanoporous graphite based on graphynes: first-principles structure and carbon dioxide preferential physisorption. ACS Appl. Mater. Interfaces **8**(41), 27996–28003 (2016). PMID: 27667472
51. Albertí, M., Aguilar, A., Cappelletti, D., Laganà, A., Pirani, F.: On the development of an effective model potential to describe ater interaction in neutral and ionic clusters. Int. J. Mass Spec. **280**, 50–56 (2009)
52. Albertí, M., Pirani, F., Laganà, A.: Carbon dioxide clathrate hydrates: selective role of intermolecular interactions and action of the SDS catalyst. J. Phys. Chem. A **117**(32), 6991–7000 (2013)
53. Lombardi, A., Pirani, F., Laganà, A., Bartolomei, M.: Energy transfer dynamics and kinetics of elementary processes (promoted) by gas-phase CO_2-N_2 collisions: selectivity control by the anisotropy of the interaction. J. Comput. Chem. **37**(16), 1463–1475 (2016)
54. Bartolomei, M., Pirani, F., Laganà, A., Lombardi, A.: A full dimensional grid empowered simulation of the CO_2 + CO_2 processes. J. Comput. Chem. **33**(22), 1806–1819 (2012)
55. Pirani, P., Brizi, S., Roncaratti, L., Casavecchia, P., Cappelletti, D., Vecchiocattivi, F.: Beyond the Lennard-Jones model: a simple and accurate potential function probed by high resolution scattering data useful for molecular dynamics simulations. Phys. Chem. Chem. Phys. **10**, 5489 (2008)
56. Lombardi, A., Laganà, A., Pirani, F., Palazzetti, F., Lago, N.F.: Carbon oxides in gas flows and earth and planetary atmospheres: state-to-state simulations of energy transfer and dissociation reactions. In: Murgante, B., et al. (eds.) ICCSA 2013. LNCS, vol. 7972, pp. 17–31. Springer, Heidelberg (2013). https://doi.org/10.1007/978-3-642-39643-4_2
57. Lago, N.F., Albertí, M., Laganà, A., Lombardi, A., Pacifici, L., Costantini, A.: The molecular stirrer catalytic effect in methane ice formation. In: Murgante, B., et al. (eds.) ICCSA 2014. LNCS, vol. 8579, pp. 585–600. Springer, Cham (2014). https://doi.org/10.1007/978-3-319-09144-0_40

58. Faginas Lago, N., Albertí, M., Lombardi, A., Pirani, F.: A force field for acetone: the transition from small clusters to liquid phase investigated by molecular dynamics simulations. Theor. Chem. Acc. **135**(7), 161 (2016)
59. Faginas-Lago, N., Albertí, M., Laganà, A., Lombardi, A.: Ion-water cluster molecular dynamics using a semiempirical intermolecular potential. In: Gervasi, O., et al. (eds.) ICCSA 2015. LNCS, vol. 9156, pp. 355–370. Springer, Cham (2015). https://doi.org/10.1007/978-3-319-21407-8_26
60. Pirani, F., Albertí, M., Castro, A., Moix Teixidor, M., Cappelletti, D.: Atom-bond pairwise additive representation for intermolecular potential energy surfaces. Chem. Phys. Lett. **394**(1–3), 37–44 (2004)
61. Pacifici, L., Verdicchio, M., Faginas-Lago, N.F., Lombardi, A., Costantini, A.: A high-level ab initio study of the $N_2 + N_2$ reaction channel. J. Comput. Chem. **34**(31), 2668–2676 (2013)
62. Faginas-Lago, N., Albertí, M., Laganà, A., Lombardi, A.: Water $(H_2O)_m$ or Benzene $(C_6H_6)_n$ aggregates to solvate the K_+? In: Murgante, B., et al. (eds.) ICCSA 2013. LNCS, vol. 7971, pp. 1–15. Springer, Heidelberg (2013). https://doi.org/10.1007/978-3-642-39637-3_1
63. Faginas-Lago, N., Lombardi, A., Albertí, M., Grossi, G.: Accurate analytic intermolecular potential for the simulation of Na^+ and K^+ ion hydration in liquid water. J. Mol. Liq. **204**, 192–197 (2015)
64. Lombardi, A., Faginas-Lago, N., Gaia, G., Federico, P., Aquilanti, V.: Collisional energy exchange in CO_2–N_2 Gaseous mixtures. In: Gervasi, O., et al. (eds.) ICCSA 2016. LNCS, vol. 9786, pp. 246–257. Springer, Cham (2016). https://doi.org/10.1007/978-3-319-42085-1_19
65. Albertí, M., Faginas-Lago, N.: Ion size influence on the Ar solvation shells of $M^+C_6F_6$ clusters (M = Na, K, Rb, Cs). J. Phys. Chem. A **116**(12), 3094–3102 (2012)
66. Aquilanti, V., Beddoni, A., Cavalli, S., Lombardi, A., Littlejohn, R.: Collective hyperspherical coordinates for polyatomic molecules and clusters. Mol. Phys. **98**(21), 1763–1770 (2000)
67. Aquilanti, V., Beddoni, A., Lombardi, A., Littlejohn, R.: Hyperspherical harmonics for polyatomic systems: basis set for Kinematic rotations. Int. J. Quantum Chem. **89**(4), 277–291 (2002)
68. Aquilanti, V., Lombardi, A., Littlejohn, R.: Hyperspherical harmonics for polyatomic systems: basis set for collective motions. Theoret. Chem. Acc. **111**(2–6), 400–406 (2004)
69. Sevryuk, M.B., Lombardi, A., Aquilanti, V.: Hyperangular momenta and energy partitions in multidimensional many-particle classical mechanics: the invariance approach to cluster dynamics. Phys. Rev. A **72**(3), 033201 (2005)
70. Smith, W., Yong, C., Rodger, P.: `DL_POLY`: application to molecular simulation. Mol. Simul. **28**(5), 385–471 (2002)
71. Elliott, J., Lira, C.T.: Introductory Chemical Engineering Thermodynamics. Prentice Hall, New Jersey (2012)
72. Humphrey, W., Dalke, A., Schulten, K.: VMD: visual molecular dynamics. J. Mol. Graph. **14**(1), 33–38 (1996)